

Comparison of posttherapy ^{90}Y positron emission tomography/computed tomography dosimetry methods in liver therapy with ^{90}Y microspheres

ABSTRACT

The aim of our study was to compare dosimetry methods for yttrium-90 (^{90}Y) positron emission tomography/computed tomography (PET/CT). Twenty-five patients were taken to a PET/CT suite following therapy with ^{90}Y microspheres. The low mA, nondiagnostic CT images were used for attenuation correction and localization of the ^{90}Y microspheres. The acquisition time was 15 min, the reconstruction matrix size was 200 mm 200 mm 75 mm, and voxel size was 4.07 mm 4.07 mm 3.00 mm. Two software packages, MIM 6.8 and Planet Dose, were utilized to calculate ^{90}Y dosimetry. Three methods were used for voxel-based dosimetry calculations: the local deposition method (LDM), LDM with scaling (LDMwS) for known injected activity, and a dose point kernel (DPK) method using the MIRK kernel. Only the DPK approach was applied to the Planet Dose software. LDM and LDMwS were only applied to the MIM software. The average total liver dosimetry values (mean \pm standard deviation) were 60.93 \pm 28.62 Gy, 53.59 \pm 23.47 Gy, 55.33 \pm 24.80 Gy, and 54.25 \pm 23.70 Gy for LDMwS, LDM, DPK with MIM, and DPK with Planet Dose (DOSI), respectively. In most cases, the LDMwS method produced slightly higher dosimetry values than the other methods. The MIM and Planet Dose DPK dosimetry values (i.e., DPK vs. DOSI) were highly comparable. Bland–Altman analysis calculated a mean difference of 1.1 \pm 2.2 Gy. The repeatability coefficient was 4.4 (7.9% of the mean). The MIM and Planet Dose DPK dosimetry values were practically interchangeable. ^{90}Y dosimetry values obtained by all methods were similar, but LDMwS tended to produce slightly higher values.

Keywords: ^{90}Y dosimetry, ^{90}Y microspheres, hepatocellular carcinoma

INTRODUCTION

Only about 20% of patients with hepatocellular carcinoma (HCC) are candidates for surgical treatment in the form of resection or transplantation, primarily due to extensive disease or other contraindications. For the remaining cases of unresectable HCC, there are many alternative treatment options, including systematic chemotherapy (e.g., sorafenib), alcohol injections, transarterial chemoembolization,^[1] thermal radiofrequency^[2] or microwave ablation, external beam radiation, and yttrium-90 (^{90}Y) radioembolization (RE).^[3] Recently, there is a growing interest in the use of RE, because of its good toxicity profile, even in patients with advanced liver cirrhosis, as well as encouraging data for time-to-progression and overall survival.^[4] In addition, the intra-arterial injection of ^{90}Y microspheres, if properly performed, delivers high-radiation doses to the tumor while sparing liver parenchyma.

Before the ^{90}Y RE itself, a mapping scan is performed using $^{99\text{m}}\text{Tc}$ macroaggregated albumin (MAA) single-photon-emission computed tomography/computed tomography (SPECT/CT), mimicking ^{90}Y distribution. Its purpose is to assess lung shunting, exclude extrahepatic deposition, and assess intrahepatic distribution. In addition, some centers are using MAA scans for personalized dosimetry calculations,


KARIN KNEŠAUREK

Department of Radiology, Icahn School of Medicine at Mount Sinai, New York, USA

Address for correspondence: Dr. Karin Knešaurek, Department of Radiology, Icahn School of Medicine at Mount Sinai, Box 1141, 1 Gustave L. Levy Place, New York, NY 10029, USA. E-mail: karin.knesaurek@mssm.edu

Submitted: 27-Feb-2020, **Revised:** 13-May-2020,

Accepted: 17-May-2020, **Published:** 22-Aug-2020

Access this article online	
Website: www.wjnm.org	Quick Response Code 
DOI: 10.4103/wjnm.WJNM_23_20	

This is an open access journal, and articles are distributed under the terms of the Creative Commons Attribution-NonCommercial-ShareAlike 4.0 License, which allows others to remix, tweak, and build upon the work non-commercially, as long as appropriate credit is given and the new creations are licensed under the identical terms.

For reprints contact: WKHLRPMedknow_reprints@wolterskluwer.com

How to cite this article: Knešaurek K. Comparison of posttherapy ^{90}Y positron emission tomography/computed tomography dosimetry methods in liver therapy with ^{90}Y microspheres. World J Nucl Med 2020;19:359-65.

assuming perfect matching between MAA and ⁹⁰Y distribution.^[5] However, there are several factors that can alter these dosimetry calculations, such as, differences in catheter positioning between MAA and ⁹⁰Y studies, differences between prepared and prescribed activities, and differences between prescribed and administered activities.^[6,7] In addition, ^{99m}Tc MAA particles and ⁹⁰Y microspheres have different flow characteristics due to differing particle sizes, dissociation, amount of particles, and embolizing effect. Therefore, the true ⁹⁰Y distribution and dosimetry can only be obtained posttherapy using bremsstrahlung SPECT (bSPECT) or positron emission tomography (PET) imaging.^[8] The importance of posttherapy ⁹⁰Y imaging is two-fold. First, it is used to detect possible extrahepatic activity, which can cause serious complications, such as ulceration and gastrointestinal bleeds.^[9-11] Second, it can be used to estimate the absorbed radiation dose delivered to liver tumors and normal liver tissue. These data can help determine whether patients' adverse events, treatment successes, or treatment failures can be attributed to the dose that the tumor or normal liver received; they are also expected to be an important predictor of treatment efficacy.^[12]

Quantitative bSPECT imaging is challenging due to scatter, septal penetration, the continuous nature of the bremsstrahlung energy spectrum, and inefficient bremsstrahlung production.^[13] Posttherapy PET ⁹⁰Y images are far superior, both qualitatively and quantitatively, to bSPECT ⁹⁰Y images.^[14]

For many years, RE with ⁹⁰Y microspheres has been primarily a palliative treatment, so large uncertainties in absorbed dose calculations have been clinically acceptable. However, recent reports on the correlation of tumor-absorbed dose with tumor response and patient survival have demonstrated the therapeutic benefit of RE beyond palliation.^[15,16] Therefore, more precise personalized, voxel-based dosimetry methods, based on quantitative imaging, are necessary to replace semi-quantitative dosimetry methods provided by vendors.^[6,7]

In this retrospective study, the aim was to compare personalized, voxel-based dosimetry methods for ⁹⁰Y PET/CT imaging using two commercially available software packages.

METHODOLOGY

Patient characteristics

This study included 25 patients (22 males and 3 females, mean age of 66.5 ± 9.7 years) with unresectable HCC who underwent RE with ⁹⁰Y microspheres at our institution from July 2014 to December 2017. All patients had negligible lung shunting

(i.e., less than 5%) and no extrahepatic leakage. Twenty patients were treated with TheraSphere® (glass microspheres; BTG, London, UK) and five with SIR-Sphere® (resin microspheres; Sirtex Medical, Sydney, Australia). All patients gave written informed consent to treatment and to retrospective analysis of their clinical and imaging data for research purposes. All procedures were performed in accordance with the ethical standards of the institutional and national research committee and the Declaration of Helsinki.

Acquisition and reconstruction protocols

In this retrospective study, the patients were taken for PET/CT imaging, following RE with ⁹⁰Y microspheres. They were imaged on a four-ring, time-of-flight (TOF) PET/CT system Biograph mCT (Siemens Medical Systems, Erlangen, Germany). Only one-bed position acquisitions were used, due to relatively long axial field of view.^[17] The low mA, nondiagnostic CT images were used for attenuation correction and localization of the ⁹⁰Y microspheres. The acquisition time was 15 min. The reconstruction matrix size was $200 \times 200 \times 75$, and the voxel size was $4.07 \text{ mm} \times 4.07 \text{ mm} \times 3.00 \text{ mm}$. ⁹⁰Y PET imaging is possible because there are 32 pair-productions per million ⁹⁰Y decays and the number of true events is low. Therefore, the lutetium oxyorthosilicate and bremsstrahlung random coincidences are often a large fraction of the prompt coincidences.^[18] In order to deal with such unfavorable situation, the iterative three-dimensional (3D) Poisson-ordered subset expectation-maximization algorithm with point spread function and TOF correction is used for reconstruction of PET data,^[19] with 2 iterations, 21 subsets (2i21s), and a 5-mm Gaussian postreconstruction filter.^[20]

Dosimetry calculation

In clinical settings worldwide, dosimetry for ⁹⁰Y RE is typically calculated using simple, semi-quantitative software provided by vendors. For those done using SIR-Spheres, the body surface area (BSA) method is primarily used;^[6] for TheraSphere treatments, activity in GBq is given as a product of dose (Gy) and mass (kg), divided by 50.^[7] A recent comparison between BSA versus personalized, voxel-based dosimetry^[21] concluded that higher activities could be administered using the voxel-based approach. In addition, tumor dosimetry (whether in terms of average dose or dose-volume histogram (DVH) metrics) was markedly associated with tumor response. These conclusions, as well as the fact that ⁹⁰Y RE is increasingly being used as a therapeutic intervention beyond palliative treatment, are going to require dosimetry tools and reference levels that allow us to better personalize treatments.^[21]

Available personalized dosimetry methods include the direct Monte Carlo (MC) simulation and dose point kernel (DPK) convolution method.^[22] Direct MC methods can take into

account both radionuclide and tissue density distributions, presumably leading to an accurate absorbed dose distribution assessment. However, in clinical practice, MC methods are not typically used, due to their complicated and lengthy calculation process. To speed up the computation, DPK approaches are preferred in clinical practice. The original DPK method was later extended to voxel sources (dose voxel kernel) in MIRD pamphlet 17^[23] by the introduction of voxel S values.

Since ⁹⁰Y decays almost entirely with β⁻ emission (0.93 MeV mean energy, half-life 64.1 h, 2.5 mm mean tissue penetration),^[24] the local deposition method (LDM) is a practical alternative to a more complicated DPK convolution approach. LDM comes in two varieties: original LDM and LDM with scaling (LDMwS) for known injected activity. In RE with ⁹⁰Y, activity before and residual activity after the treatment are always measured, providing the net activity injected into the patient's liver. Then, the total counts in the PET image can be scaled with net activity, providing corrected quantitative images used for dosimetry calculation. The scaling and corrected quantitative images are combined with LDM producing the LDMwS variant. Original LDM and DPK use PET calibration data to obtain quantifiable images and to calculate voxel-based dosimetry. Two commercially available software packages, Planet Dose (DOSIsoft SA, Cachan, France) [Figure 1] and MIM 6.8 (MIM Software Inc., Cleveland, Ohio, USA) [Figure 2], were utilized to calculate ⁹⁰Y dosimetry from the PET images.

The Planet Dose software and the MIM software can use DPK, LDM, and LDMwS dosimetry calculations; however, in

this study, only the DPK approach was applied to the Planet Dose software. These values were compared with MIM DPK dosimetry values. The DPK method can be used for both γ and β⁻ radionuclides, while LDM and LDMwS can only be used for short-range radionuclides such as ⁹⁰Y, which is almost pure β⁻ emitter. The DPK approach is assumed to be superior to the LDM because LDM does not take into account cross-talk between different voxels. The LDM approach assumes that all radiation energy is deposited within one voxel, due to the limited range of β⁻ emission. In this study, LDM and LDMwS were only applied to the MIM software in order to compare different dosimetry approaches, i.e., an approach using direct PET quantification imaging versus one using scaling corrected quantifiable images.

Statistical analyses

A Passing–Bablok regression scatter diagram was used to compare dosimetry values obtained from each of the methods, displaying the regression line (solid line), the confidence intervals for the regression line (dashed lines), and the identity line (x = y, dotted line).^[25] A Spearman rank correlation coefficient (ρ) was also reported. The Bland and Altman method^[26] was used to analyze the difference between the dosimetry values obtained by each approach and to test the repeatability of these results. The repeatability coefficient was calculated as 1.96 times the standard deviation (SD) of the differences.^[27] The dosimetry data were reported as mean ± SD. For comparison, the repeatability coefficient was also given as a percentage of the average values of the doses obtained by these two approaches. The statistical analysis was performed using

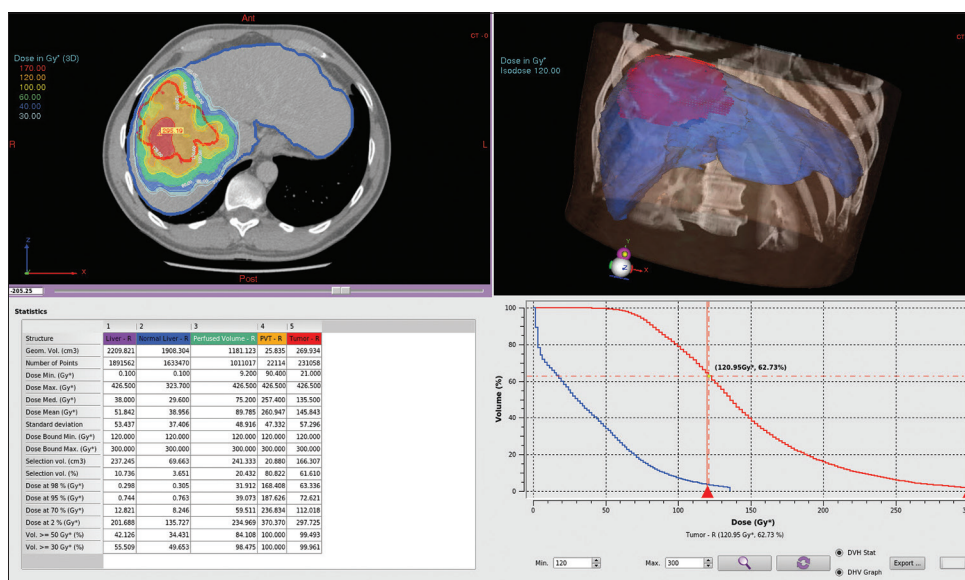


Figure 1: Computed tomography liver image, showing creation of ROIs in transaxial slices and visualized in three-dimensional display using Planet Dose (DOSIsoft SA, Cachan, France) dosimetry software. The software provides volumes and mean, maximal, and minimal dosimetry values, as well as DVH and isodose curves for total liver, tumors, and normal tissue

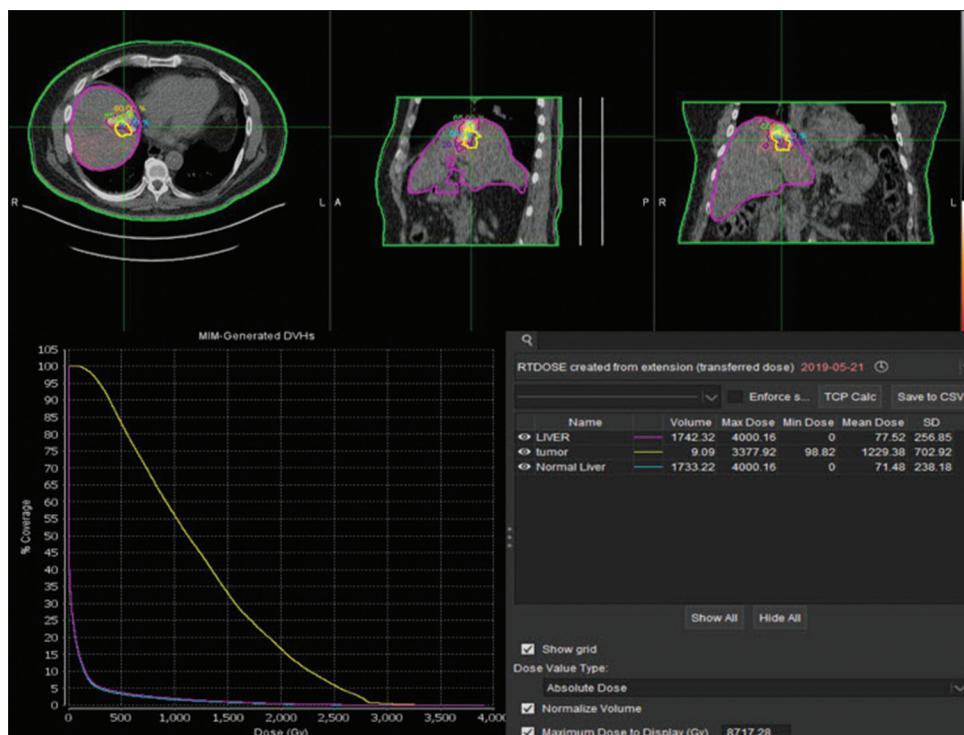


Figure 2: Computed tomography liver images, showing creation of ROIs in transaxial slices, and visualized in sagittal and axial slices using MIM 6.8 (MIM Software Inc., Cleveland, Ohio) software. The body contour in computed tomography liver slices was used to create body VOI in order to scale net injected ^{90}Y activity and used for local deposition method with scaling dosimetry method

MedCalc Software (MedCalc, bvba 17– 64 bit version, Ostend, Belgium).

RESULTS

The mean liver doses calculated using DPK with MIM versus DPK with Planet Dose (DOSI) (i.e., DPK vs. DOSI) were similar, coming out to 55.33 ± 24.80 Gy and 54.25 ± 23.70 Gy, respectively, with a mean difference of 1.1 ± 2.2 Gy. The repeatability coefficient was 4.4 (7.9% of the mean) and the Spearman rank correlation coefficient was high ($\rho = 0.99$) [Figure 3]. The mean liver doses calculated using LDM versus DPK were also similar, coming out to 53.59 ± 23.47 Gy, and 55.33 ± 24.80 Gy, respectively, with a mean difference of -1.7 ± 2.0 Gy. The repeatability coefficient was 3.9 (7.2% of the mean) and the Spearman rank correlation coefficient was high ($\rho = 0.99$) [Figure 4]. The mean liver doses calculated using LDMwS versus LDM were 60.93 ± 28.62 Gy and 53.59 ± 23.47 Gy, respectively, with a mean difference of 7.3 ± 6.7 Gy. The repeatability coefficient was 13.2 (23.0% of the mean) and the Spearman rank correlation coefficient was high ($\rho = 0.98$) [Figure 5]. Other dosimetry comparisons, such as LDM vs. DOSI and LDMwS vs. DOSI, are not provided because a comparison between LDM, DPK, and DOSI showed that the results were very close. A comparison of all dosimetry combinations calculations was plotted [Figure 6], and the average total liver dosimetry values

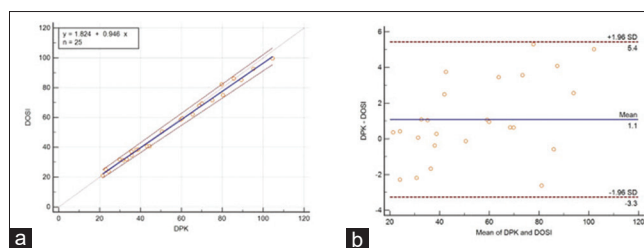


Figure 3: (a) The Passing–Bablok regression scatter diagram with the regression line (solid line), the confidence interval for regression line (dashed lines), and identity line ($x = y$, dotted line) for mean liver dose values in Gy obtained from DOSI and DPK methods and all 25 patients. The Spearman rank correlation coefficient was high ($\rho = 0.99$). (b) Bland–Altman plot for all 25 patients, with a mean difference of 1.1 ± 2.2 Gy. The repeatability coefficient was 4.4 (7.9% of the mean). DPK: Dose point kernel

were 60.93 ± 28.62 Gy, 53.59 ± 23.47 Gy, 55.33 ± 24.80 Gy, and 54.25 ± 23.70 Gy for LDMwS, LDM, DPK, and DOSI, respectively.

DISCUSSION

Two dosimetry approaches were compared in this study. The first approach used the calibration properties of the PET system to obtain the activity per voxel in posttherapy images. From these activities, DPK or LDM was used to calculate dosimetry values for each pixel, ultimately providing tumor, normal liver parenchyma, and total liver dosimetry values. The second approach used the known net activity administered to the

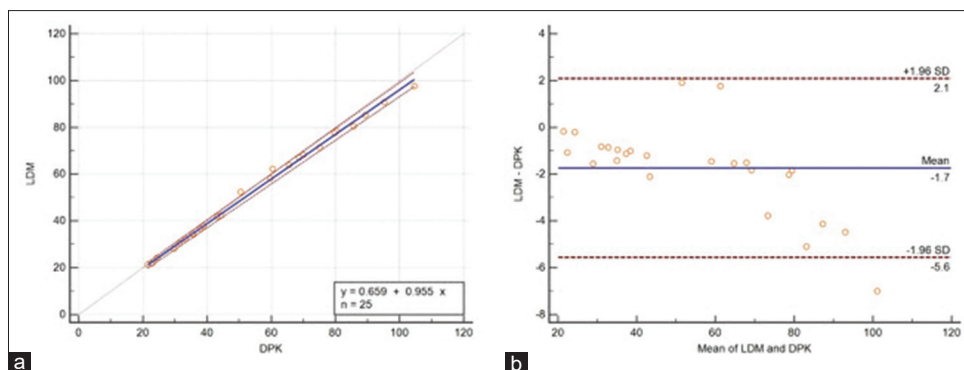


Figure 4: (a) The Passing–Bablok regression scatter diagram with the regression line (solid line), the confidence interval for regression line (dashed lines), and identity line ($x = y$, dotted line) for mean liver dose values in Gy obtained from LDM and DPK methods and all 25 patients. The Spearman rank correlation coefficient was high ($\rho = 0.99$). (b) Bland–Altman plot for all 25 patients, with a mean difference of -1.7 ± 2.0 Gy. The repeatability coefficient was 3.9 (7.2% of the mean). LDM: Local deposition method, DPK: Dose point kernel

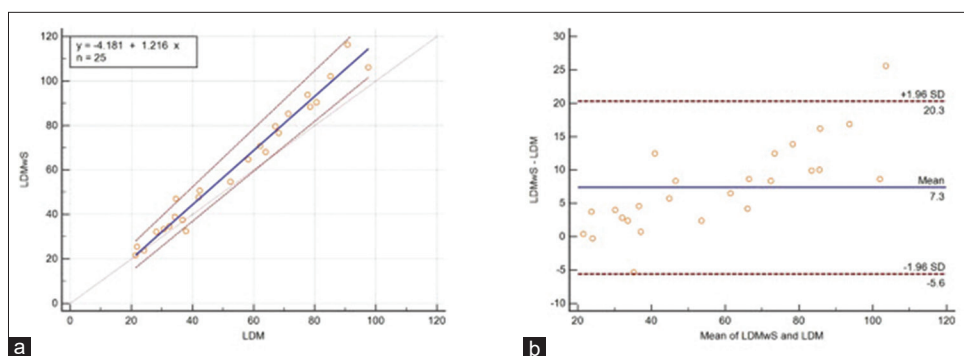


Figure 5: (a) The Passing–Bablok regression scatter diagram with the regression line (solid line), the confidence interval for regression line (dashed lines), and identity line ($x = y$, dotted line) for mean liver dose values in Gy obtained from LDMwS and LDM methods and all 25 patients. The Spearman rank correlation coefficient was high ($\rho = 0.98$). (b) Bland–Altman plot for all 25 patients, with a mean difference of 7.3 ± 6.7 Gy. The repeatability coefficient was 13.2 (23.0% of the mean). LDM: Local deposition method, LDMwS: LDM with scaling

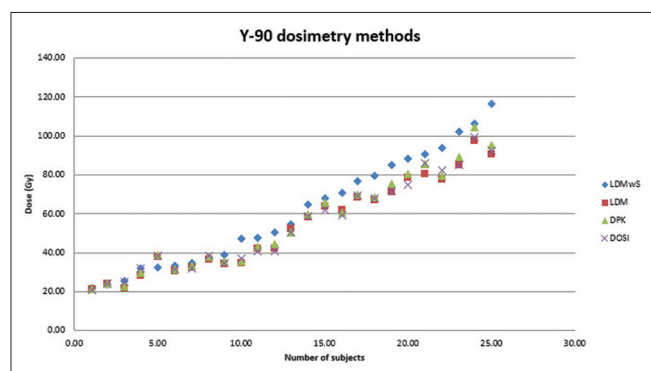


Figure 6: Comparison of all dosimetry methods. The average total liver dosimetry values were 60.93 ± 28.62 Gy, 53.59 ± 23.47 Gy, 55.33 ± 24.80 Gy, and 54.25 ± 23.70 Gy for LDMwS, LDM, DPK, and DOSI, respectively. While, LDM, DPK, and DOSI dosimetry values were very close, Y-90 dosimetry values obtained by LDMwS tended to produce slightly higher values. LDM: Local deposition method, DPK: Dose point kernel, LDMwS: LDM with scaling

patient, which was then scaled according to the distribution of counts in the 3D reconstructed posttherapy images. LDMwS was then used to calculate dosimetry values for tumor, normal liver parenchyma, and total liver in posttherapy studies. The advantage of the first approach is that it does not require

posttherapy residual activity measurements. The advantage of the second approach is that it can be used on a noncalibrated system such as bremsstrahlung SPECT imaging.^[28]

The commercially available software packages, MIM 6.8 (MIM Software Inc., Cleveland, Ohio, USA) and Planet Dose (DOSIsoft SA, Cachan, France), are similar but do have some small differences. Both strongly recommend using a 2D brush for creation of transaxial regions-of-interest (ROIs). From a stack of transaxial 2D ROIs, one can create a full 3D volume of interest (VOI) of the liver, tumors, and normal liver parenchyma. The Planet Dose software is made by the primarily radiation therapy (RT) company, with strong commitment to dosimetry calculations for external and internal radiation treatment planning. Their 2D brush can distinguish well between lung and upper liver tissue, improving the efficiency of creating ROIs for that body area. They also have very nice 3D presentation of the liver and inserted tumor tissue. On the other hand, MIM software has an excellent customer support providing different workloads, as required by different institutions

with differing preferences. Furthermore, MIM software can interpolate between transaxial slices during the process of VOI creation. Planet Dose software can do the same but only after finishing all axial 2D ROIs, and any corrections can be done on the full 3D VOI. Both software packages can provide mean, maximal, and minimal dose values in Gy and provide DVH for total liver, tumors, and normal liver. Furthermore, as full 3D voxel-based dosimetry packages, both software applications provide isodose curves.

Suggested improvements for both software packages include a full 3D brush possibility, which would allow direct creation of VOIs. Furthermore, the addition of a liver atlas would be useful for easier liver delineation. Some such attempts have been made, but the creation of liver VOI is still primarily done manually in clinical practice. This step is the most time-consuming part of dosimetry calculation in RE with ⁹⁰Y. The most desirable solution would be a fully automatic creation of liver, tumors, and normal liver VOIs using artificial intelligence methods, such as deep convolution neural networks.^[29] This advancement would make dosimetry calculations in RE with ⁹⁰Y significantly more efficient and more appealing in clinical practice.

Our results showed that DPK dosimetry values produced by each dosimetry software programs (i.e., DPK vs. DOSI) were practically identical. Furthermore, LDM and DPK results were very similar, confirming that for ⁹⁰Y, which is almost 100% a β^- emitter, LDM can be used for dosimetry calculations. The results also indicate that the LDMwS had slightly higher values in comparison to LDM and DPK [Figure 6]. A previous phantom study^[30] revealed a similar trend. Our understanding is that the slightly higher values produced by LDMwS compared to the other methods are due to the difference between dose calibrator scaling, as well as the quantitative accuracy of ⁹⁰Y PET imaging. This comes down to a choice between using direct quantifiable PET images versus scaled and corrected images using dose calibrator values. Although the differences are not great, they should be diminished by improved quantifiable ⁹⁰Y PET imaging and dose calibrator quality control.

CONCLUSIONS

In addition to palliative treatment, RE with ⁹⁰Y microspheres is increasingly being used as a therapeutic intervention. Therefore, more precise personalized, voxel-based dosimetry methods based on quantitative imaging are necessary to replace semi-quantitative dosimetry methods. Our results indicate that DPK dosimetry values produced by each dosimetry software programs (i.e., DPK vs. DOSI) were

practically identical. Small differences can be attributed to differing methods in the creation of regions of interest. LDM and DPK dosimetry values were also very similar, while ⁹⁰Y dosimetry values obtained by LDMwS tended to produce slightly higher values. Improved quantifiable ⁹⁰Y PET imaging and dose calibrator quality control should minimize differences between LDMwS on one side with LDM and DPK dosimetry methods.

Acknowledgment

We thank Dr. Sebastien Vauclin, DOSIsoft SA, Cachan, France, for his valuable comments.

Financial support and sponsorship

Nil.

Conflicts of interest

There are no conflicts of interest.

REFERENCES

1. Lobo L, Yakoub D, Picado O, Ripat C, Pendola F, Sharma R, *et al.* Unresectable hepatocellular carcinoma: Radioembolization versus chemoembolization: A systematic review and meta-analysis. *Cardiovasc Intervent Radiol* 2016;39:1580-8.
2. Sucandy I, Cheek S, Golas BJ, Tsung A, Geller DA, Marsh JW. Long term survival outcomes of patients undergoing treatment with radiofrequency ablation for hepatocellular carcinoma and metastatic colorectal cancer liver tumors. *HPB J Int Hepato Pancreato Biliary Assoc* 2016;18:756-63.
3. Paprottka PM, Hoffmann RT, Haug A, Sommer WH, Raessler F, Trumm CG, *et al.* Radioembolization of symptomatic, unresectable neuroendocrine hepatic metastases using yttrium-90 microspheres. *Cardiovasc Intervent Radiol* 2012;35:334-42.
4. Hilgard P, Hamami M, El Fouly A, Scherag A, Müller S, Ertle J, *et al.* Radioembolization With yttrium-90 Glass Microspheres in Hepatocellular Carcinoma: European Experience on Safety and Long-Term Survival. *Hematology* 2010;52:1741-9.
5. Garin E, Rolland Y, Laffont S, Edeline J. Clinical impact of (99m) Tc-MAA SPECT/CT-based dosimetry in the radioembolization of liver malignancies with (90)Y-loaded microspheres. *Eur J Nucl Med Mol Imaging* 2016;43:559-75.
6. The Package Insert for SIR-Spheres® Y-90 resin microspheres. Sirtex Medical Limited; 2018. Available from: <https://www.sirtex.com/media/155127/pi-ec-12.pdf>. [Last accessed on 2020 Apr 03].
7. TheraSphere Package Insert. BTG; 2018. Available from: https://www.btg-im.com/BTG/media/TheraSphere-Documents/PDF/TheraSphere-Package-Insert_USA_Rev-14.pdf. [Last accessed on 2019 Mar 15].
8. Knešaurek K, Kim E, Livnat U, Eldib M, Fayad Z, Kostakoglu L. Comparison of Y-90 dosimetry derived from post-therapy PET/CT and PET/MRI imaging. *J Nucl Med* 2016;57:1294.
9. Murthy R, Brown DB, Salem R, Meranze SG, Coldwell DM, Krishnan S, *et al.* Gastrointestinal complications associated with hepatic arterial Yttrium-90 microsphere therapy. *J Vasc Interv Radiol* 2007;18:553-61.
10. Riaz A, Lewandowski RJ, Kulik LM, Mulcahy MF, Sato KT, Ryu RK, *et al.* Complications following radioembolization with yttrium-90 microspheres: A comprehensive literature review. *J Vasc Interv Radiol*

- 2009;20:1121-30.
11. Ahmadzadehfar H, Muckle M, Sabet A, Wilhelm K, Kuhl C, Biermann K, *et al.* The significance of bremsstrahlung SPECT/CT after yttrium-90 radioembolization treatment in the prediction of extrahepatic side effects. *Eur J Nucl Med Mol Imaging* 2012;39:309-15.
 12. Chiesa C, Maccauro M, Romito R, Spreafico C, Pellizzari S, Negri A, *et al.* Need, feasibility and convenience of dosimetric treatment planning in liver selective internal radiation therapy with Y-90 microspheres: The experience of the National Cancer Institute of Milan. *Q J Nucl Med Mol Imaging* 2011;55:168-97.
 13. Knešaurek K, Tuli A, Kim E, Kostakoglu L. Comparison of Y-90 dosimetry derived from post-therapy PET/CT and bremsstrahlung SPECT imaging. *J Nucl Med* 2016;57:1893.
 14. Elschot M, Vermolen BJ, Lam MG, de Keizer B, van den Bosch MA, de Jong HW. Quantitative comparison of PET and bremsstrahlung SPECT for imaging *in vivo* Yttrium-90 microsphere distribution after liver radioembolization. *PLoS One* 2013;8:E55742.
 15. Kappadath SC, Mikell J, Balagopal A, Baladandayuthapani V, Kaseb A, Mahvash A. Hepatocellular Carcinoma Tumor Dose Response After ^{90}Y -radioembolization With Glass Microspheres Using Y-SPECT/CT-Based Voxel Dosimetry. *Int J Radiat Oncol Biol Phys* 2018;102:451-61.
 16. Levillain H, Derijckere ID, Marin G, Guiot T, Vouche M, Reynaert N, *et al.* Y-90-PET/CT based dosimetry after selective internal radiation therapy predicts outcome in patients with liver metastases from colorectal cancer. *EJNMMI Res* 2018;8:1-9.
 17. Knešaurek K, Tuli A, Kim E, Heiba S, Kostakoglu L. Comparison of PET/CT and PET/MR imaging and dosimetry of yttrium-90 (Y-90) in patients with unresectable hepatic tumors who have received intra-arterial radioembolization therapy with Y-90 microspheres. *EJNMMI Phys* 2018;5:23.
 18. Goedicke A, Berker Y, Verburg FA, Behrend FF, Winz O, Mottaghy FM. Study-parameter impact in quantitative 90-Yttrium PET imaging for radioembolization treatment monitoring and dosimetry. *IEEE Trans Med Imaging* 2013;32:485-92.
 19. Carlier T, Willowson KP, Fourkal E, Bailey DL, Doss M, Conti M. Y-90 -PET imaging: Exploring limitations and accuracy under conditions of low counts and high random fraction. *Med Phys* 2015;42:4295-309.
 20. Willowson KP, Tapner M, Bailey DL. A multicentre comparison of quantitative Y-90 PET/CT for dosimetric purposes after radioembolization with resin microspheres: The QUEST Phantom Study. *Eur J Nucl Med Mol Imaging* 2015;42:1202-22.
 21. Kafrouni M, Allimant C, Fourcade M, Vauclin S, Delicque J, Ilonca AD, *et al.* Retrospective voxel-based dosimetry for assessing the body surface area model ability to predict delivered dose and radioembolization outcome. *J Nucl Med* 2018;59:1289-95.
 22. Dieudonné A, Hobbs RF, Lebtahi R, Maurel F, Baechler S, Wahl RL, *et al.* Study of the impact of tissue density heterogeneities on 3-dimensional abdominal dosimetry: Comparison between dose kernel convolution and direct Monte Carlo methods. *J Nucl Med* 2013;54:236-43.
 23. Bolch WE, Bouchet LG, Robertson JS, Wessels BW, Siegel JA, Howell RW, *et al.* MIRD pamphlet no. 17: The dosimetry of nonuniform activity distributions – Radionuclide S values at the voxel level. Medical Internal Radiation Dose Committee. *J Nucl Med* 1999;40:11S-36S.
 24. Maughan NM, Eldib M, Conti M, Knešaurek K, Faul D, Parikh PJ, *et al.* Phantom study to determine optimal PET reconstruction parameters for PET/MR imaging of Y-90 microspheres following radioembolization. *Biomed Phys Eng Express* 2016;2:15009.
 25. Passing H, Bablok W. A new biometrical procedure for testing the equality of measurements from two different analytical methods. Application of linear regression procedures for method comparison studies in Clinical Chemistry, Part I. *J Clin Chem Clin Biochem* 1983;21:709-20.
 26. Bland JM, Altman DG. Statistical methods for assessing agreement between two methods of clinical measurement. *Lancet* 1986;327:307-10.
 27. Precision of Test Methods. I: Guide for the Determination and Reproducibility for a Standard Test Method. London, U.K.: British Standards Institution; 1976. p. 54-97.
 28. Knešaurek K, Heiba S, Pyzik R, Pasik SD, Kostakoglu L. An estimate of Y-90 dosimetry for bremsstrahlung SPECT/CT imaging. *J Nucl Med* 2019;60 Suppl 1:124.
 29. Sibille L, Seifert R, Avramovic N, Vehren T, Spottiswoode B, Zuehlsdorf S, *et al.* ^{18}F -FDG PET/CT uptake classification in lymphoma and lung cancer by using deep convolution neural networks. *Radiology* 2020;294:445-52.
 30. Nelson A, Swallen A, Dewaraja Y. Evaluation of voxel-based yttrium-90 (Y-90) dose calculation methods for Y-90 PET using a liver phantom. *J Nucl Med* 2016; 57 Suppl 2:1424.